

Lossy Image Compression with Conditional Diffusion Models

Anonymous Authors¹

Abstract

This paper outlines an end-to-end optimized lossy image compression framework using diffusion generative models. The approach relies on the transform coding paradigm, where an image is mapped into a latent space for entropy coding and, from there, mapped back to the data space for reconstruction. In contrast to VAE-based neural compression, where the (mean) decoder is a deterministic neural network, our decoder is a conditional diffusion model. Our approach thus introduces an additional “content” latent variable on which the reverse diffusion process is conditioned and uses this variable to store information about the image. The remaining “texture” variables characterizing the diffusion process are synthesized at decoding time. We show that the model’s performance can be tuned toward perceptual metrics of interest. Our extensive experiments involving multiple datasets and image quality assessment metrics show that our approach yields stronger reported FID scores than the GAN-based model, while also yielding competitive performance with VAE-based models in several distortion metrics. Furthermore, training the diffusion with \mathcal{X} -parameterization enables high-quality reconstructions in only a handful of decoding steps, greatly affecting the model’s practicality.

1. Introduction

With visual media vastly dominating consumer internet traffic, developing new efficient codecs for images and videos has become evermore crucial (Cisco, 2017). The past few years have shown considerable progress in deep learning-based image codecs that have outperformed classical codecs in terms of the inherent tradeoff between rate (expected file size) and distortion (quality loss) (Ballé et al., 2018;

¹Anonymous Institution, Anonymous City, Anonymous Region, Anonymous Country. Correspondence to: Anonymous Author <anon.email@domain.com>.

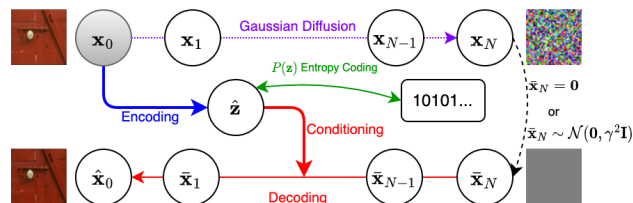


Figure 1: Overview of our proposed compression architecture. A discrete “content” latent variable \hat{z} contains information about the image. Upon decoding, this variable is used for conditioning a denoising diffusion process. The involved “texture” variables $\bar{x}_{1:N}$ are synthesized on the fly.

Minnen et al., 2018; Minnen & Singh, 2020; Zhu et al., 2021; Yang et al., 2020; Cheng et al., 2020; Yang et al., 2023). Recent research promises even more compression gains upon optimizing for perceptual quality, i.e., increasing the tolerance for imperceivable distortion for the benefit of lower rates (Blau & Michaeli, 2019). For example, adding adversarial losses (Agustsson et al., 2019; Mentzer et al., 2020) showed good perceptual quality at low bitrates.

Most state-of-the-art learned codecs currently rely on transform coding and involve hierarchical “compressive” variational autoencoders (Ballé et al., 2018; Minnen et al., 2018; Cheng et al., 2020). These models simultaneously transform the data into a lower dimensional latent space and use a learned prior model for entropy-coding the latent representations into short bit strings. Using either Gaussian or Laplacian decoders, these models directly optimize for low MSE/MAE distortion performance. Given the increasing focus on perceptual performance over distortion, and the fact that VAEs suffer from mode averaging behavior inducing blurriness (Zhao et al., 2017) suggest expected performance gains when replacing the Gaussian decoder with a more expressive conditional generative model.

This paper proposes to relax the typical requirement of Gaussian (or Laplacian) decoders in compression setups and presents a more expressive generative model instead: a conditional diffusion model. Diffusion models have achieved remarkable results on high-quality image generation tasks (Ho et al., 2020; Song et al., 2021b;a). By hybridizing hierarchical compressive VAEs (Ballé et al., 2018) with conditional diffusion models, we create a novel deep generative model

with promising properties for perceptual image compression. This approach is related to but distinct from the recently proposed Diff-AEs (Preechakul et al., 2022), which are neither variational (as needed for entropy coding) nor tailored to the demands of image compression.

We evaluate our new compression model on four datasets and investigate a total of 16 different metrics, ranging from distortion metrics, perceptual reference metrics, and no-reference perceptual metrics. We find that the approach yields the best reported performance in FID and is otherwise comparable with the best available compression models while showing more consistent behavior across the different tasks. We also show that making the decoder more stochastic vs. deterministic offers a new possibility to steer the tradeoff between distortion and perceptual quality (Blau & Michaeli, 2019). Crucially, we find that a certain parameterization— \mathcal{X} -prediction (Salimans & Ho, 2022)—can yield high-quality reconstructions in only a handful of diffusion steps.

In sum, our contributions are as follows:

- We propose a novel transform-coding-based lossy compression scheme using diffusion models. The approach uses an encoder to map images onto a contextual latent variable; this latent variable is then fed as context into a diffusion model for reconstructing the data. The approach can be modified to enhance several perceptual metrics of interest.
- We derive our model’s loss function from a variational upper bound to the diffusion model’s implicit rate-distortion function. The resulting distortion term is distinct from traditional VAEs in capturing a richer decoding distribution. Moreover, it achieves high-quality reconstructions in only a handful of denoising steps.
- We provide substantial empirical evidence that a variant of our approach is, in many cases, better than the GAN-based models in terms of perceptual quality, such as FID. Our base model also shows comparable rate-distortion performance with MSE-optimized baselines. To this end, we considered four test sets, three baseline models (Wang et al., 2022; Mentzer et al., 2020; Cheng et al., 2020), and up to sixteen image quality assessment metrics.

2. Method

2.1. Conditional Diffusion Model for Compression

The basis of our compression approach is a new latent variable model: the diffusion variational autoencoder. This model has a “semantic” latent variable \mathbf{z} for encoding the image content, and a set of “texture” variables $\mathbf{x}_{1:N}$ describ-

ing residual information,

$$p(\mathbf{x}_{0:N}, \mathbf{z}) = p(\mathbf{x}_{0:N}|\mathbf{z})p(\mathbf{z}). \quad (1)$$

As detailed below, the decoder will follow a denoising process conditioned on \mathbf{z} . We use a neural encoder $e(\mathbf{z}|\mathbf{x}_0)$ to encode the image. The prior $p(\mathbf{z})$ is a two-level hierarchical prior (commonly used in learned image compression) and is used for entropy coding \mathbf{z} after quantization (Ballé et al., 2018). Next, we discuss the novel decoder model.

Decoder and training objective We construct the conditional denoising diffusion model in a similar way to the non-variational diffusion autoencoder of Preechakul et al. (2022). We introduce a conditional denoising diffusion process for decoding the latent \mathbf{z} ,

$$\begin{aligned} p_\theta(\mathbf{x}_{0:T}|\mathbf{z}) &= p(\mathbf{x}_N) \prod p_\theta(\mathbf{x}_{n-1}|\mathbf{x}_n, \mathbf{z}) \\ &= p(\mathbf{x}_N) \prod \mathcal{N}(\mathbf{x}_{n-1}|M_\theta(\mathbf{x}_n, \mathbf{z}, n), \beta_n \mathbf{I}). \end{aligned} \quad (2)$$

Since the texture latent variables $\mathbf{x}_{1:N}$ are not compressed but synthesized at decoding time, the optimal encoder and prior should be learned jointly with the decoder’s marginal likelihood $p(\mathbf{x}_0|\mathbf{z}) = \int p(\mathbf{x}_{0:N}|\mathbf{z})d\mathbf{x}_{1:N}$ while targeting a certain tradeoff between rate and distortion specified by a Lagrange parameter λ . We can upper-bound this rate-distortion (R-D) objective by invoking Jensen’s inequality,

$$\begin{aligned} \mathbb{E}_{\mathbf{z} \sim e(\mathbf{z}|\mathbf{x}_0)} [-\log p(\mathbf{x}_0|\mathbf{z}) - \lambda \log p(\mathbf{z})] &\leq \\ \mathbb{E}_{\mathbf{z} \sim e(\mathbf{z}|\mathbf{x}_0)} [L_{\text{upper}}(\mathbf{x}_0|\mathbf{z}) - \lambda \log p(\mathbf{z})], \end{aligned}$$

where $L_{\text{upper}}(\mathbf{x}_0|\mathbf{z}) = -\mathbb{E}_{\mathbf{x}_{1:N} \sim q(\mathbf{x}_{1:N}|\mathbf{x}_0)} \left[\log \frac{p(\mathbf{x}_{0:N}|\mathbf{z})}{q(\mathbf{x}_{1:N}|\mathbf{x}_0)} \right]$ is the variational upper bound to the diffusion model’s negative data log likelihood (Ho et al., 2020). We realize that $L_{\text{upper}}(\mathbf{x}_0|\mathbf{z})$ corresponds to a novel *image distortion* metric induced by the conditional diffusion model (in analogy to how a Gaussian decoder induces the MSE distortion). This term measures the model’s ability to reconstruct the image based on \mathbf{z} . In contrast, $-\log p(\mathbf{z})$ measures the number of bits needed to compress \mathbf{z} under the prior. As in most other works on neural image compression (Ballé et al., 2018; Minnen et al., 2018; Yang et al., 2023), we use a box-shaped stochastic encoder $e(\mathbf{z}|\mathbf{x}_0)$ that simulates rounding by noise injection at training time.

We simplify the training objective by using the denoising score matching loss,

$$\begin{aligned} L_{\text{upper}}(\mathbf{x}_0|\mathbf{z}) &\approx \mathbb{E}_{\mathbf{x}_0, n, \epsilon} \left\| \epsilon - \epsilon_\theta(\mathbf{x}_n, \mathbf{z}, \frac{n}{N_{\text{train}}}) \right\|^2 = \\ &\mathbb{E}_{\mathbf{x}_0, n, \epsilon} \frac{\alpha_n}{1 - \alpha_n} \left\| \mathbf{x}_0 - \mathcal{X}_\theta(\mathbf{x}_n, \mathbf{z}, \frac{n}{N_{\text{train}}}) \right\|^2 \end{aligned} \quad (3)$$

n and α_n are noise scheduling parameters. Instead of conditioning on n , we condition the model on the pseudo-continuous variable $\frac{n}{N_{\text{train}}}$ which offers additional flexibility

in choosing the number of denoising steps for decoding (e.g., we can use a N_{test} smaller than N_{train}). The right-hand-side equation describes an alternative form of the loss function, where \mathcal{X}_θ directly learns to reconstruct \mathbf{x}_0 instead of ϵ (Salimans & Ho, 2022). We can easily derive the equivalence with $\epsilon_\theta(\mathbf{x}_n, \mathbf{z}, \frac{n}{N}) = \frac{\mathbf{x}_n - \sqrt{\alpha_n} \mathcal{X}_\theta(\mathbf{x}_n, \mathbf{z}, \frac{n}{N})}{\sqrt{1 - \alpha_n}}$.

Decoding process Once the model is trained, we entropy-decode \mathbf{z} using the prior $p(\mathbf{z})$ and conditionally decode the image \mathbf{x}_0 using ancestral sampling. We consider two decoding schemes: a stochastic one with $\mathbf{x}_N \sim \mathcal{N}(0, \gamma^2 I)$ (where $\gamma > 0$) and a deterministic version with $\mathbf{x}_N = \mathbf{0}$ (or $\gamma = 0$), both following the DDIM sampling method:

$$\mathbf{x}_{n-1} = \sqrt{\alpha_{n-1}} \mathcal{X}_\theta(\mathbf{x}_n, \mathbf{z}, \frac{n}{N}) + \sqrt{1 - \alpha_{n-1}} \epsilon_\theta(\mathbf{x}_n, \mathbf{z}, \frac{n}{N}) \quad (4)$$

Since the variables $\mathbf{x}_{1:N}$ are not stored but generated at test time, these ‘‘texture’’ variables can result in variable reconstructions upon stochastic decoding (see Figure 5 for decoding with different γ).

Fast decoding using \mathcal{X} -prediction In most applications of diffusion models, the iterative generative process is a major roadblock towards fast generation. Although various methods have been proposed to reduce the number of iterations, they often require additional post-processing methods, such as progress distillation (Salimans & Ho, 2022) and parallel denoising (Zheng et al., 2022).

Surprisingly, in our use case of diffusion models, we found that the \mathcal{X} -prediction model with *only a handful of decoding steps* achieves comparable compression performance to the ϵ -model with hundreds of steps, without the need of any post-processing. This can be explained by closely inspecting \mathcal{X} -prediction objective from Eq. 3 that almost looks like an autoencoder loss, with the modification that n and \mathbf{x}_n are given as additional inputs. When n is large, \mathbf{x}_n looks like pure noise and doesn’t contain much information about \mathbf{x}_0 ; in this case, \mathcal{X} will ignore this input and reconstruct the data based on the content latent variable \mathbf{z} . In contrast, if n is small, \mathbf{x}_n will closely resemble \mathbf{x}_0 and hence carry *more* information than \mathbf{z} to reconstruct the image. This is to say that our diffusion objective inherits the properties of an autoencoder to reconstruct the data in a single iteration; however, successive decoding allows the model to refine this estimate and arrive at a reconstruction closer to the data manifold, with beneficial effects for perceptual properties.

Optional Perceptual Loss While Eq. 3 already describes a viable loss function for our conditional diffusion compression model, we can influence the perceptual quality of the compressed images by introducing additional loss functions similar to (Mentzer et al., 2020).

First, we note that the decoded data point can be under-

stood as a function of the low-level latent \mathbf{x}_n , the latent code \mathbf{z} , and the iteration n , such that $\bar{\mathbf{x}}_0 = \mathcal{X}_\theta(\mathbf{x}_n, \mathbf{z}, n/N)$ or $\frac{\mathbf{x}_n - \sqrt{1 - \alpha_n} \epsilon_\theta(\mathbf{x}_n, \mathbf{z}, n/N)}{\sqrt{\alpha_n}}$. When minimizing a perceptual metric $d(\cdot, \cdot)$, we can therefore add a new term to the loss:

$$L_p = \mathbb{E}_{\epsilon, n, \mathbf{z} \sim e(\mathbf{z}|\mathbf{x}_0)} [d(\bar{\mathbf{x}}_0, \mathbf{x}_0)] \quad (5)$$

$$L_c = \mathbb{E}_{\mathbf{z} \sim e(\mathbf{z}|\mathbf{x}_0)} [L_{\text{upper}}(\mathbf{x}_0|\mathbf{z}) - \frac{\lambda}{1 - \rho} \log p(\mathbf{z})] \quad (6)$$

$$L = \rho L_p + (1 - \rho) L_c. \quad (7)$$

This loss term is weighted by an additional Lagrange multiplier $\rho \in [0, 1]$, resulting in a three-way tradeoff between rate, distortion, and perceptual quality (Yang et al., 2023).

We stress that different variations of perceptual losses for compression have been proposed (Yang et al., 2023). While this paper uses the widely-adopted LPIPS loss (Zhang et al., 2018), other approaches add an adversarial term that seek to make the reconstructions indistinguishable from reconstructed images. In this setup, Blau & Michaeli (2019) have proven mathematically that it is impossible to simultaneously obtain arbitrarily good perceptual qualities and low distortions. In this paper, we observe a similar fundamental tradeoff between perception and distortion.

3. Experiments

We conducted a large-scale compression evaluation involving multiple image quality metrics and test datasets. Besides metrics measuring the traditional distortion scores, we also consider metrics that can reflect perceptual quality. While some of these metrics are fixed, others are learned from data. We will refer to our approach as ‘‘Conditional Diffusion Compression’’ (CDC). We selected sixteen metrics for image quality evaluations, of which we present eight most widely-used ones in the main paper.

3.1. Baseline Comparisons

Baselines and Model Variants We showed two variants of our \mathcal{X} -prediction CDC model. Our first proposed model is optimized in the presence of an additive perceptual reconstruction term at $\rho = 0.9$, which is the largest ρ -value we chose. For this variant, we used $\mathbf{x}_N \sim \mathcal{N}(0, \gamma^2 I)$ with $\gamma = 0.8$ to reconstruct the images. The other proposed version is the base model, trained without the additional perceptual term ($\rho = 0$) and using a deterministic decoding with $\mathbf{x}_N = \mathbf{0}$. As discussed below, this base version performs better in terms of distortion metrics, while the stochastic and LPIPS-informed version performs better in perceptual metrics.

We compare our method with several neural compression methods. The best reported perceptual results were obtained by HiFiC (Mentzer et al., 2020). This model is optimized

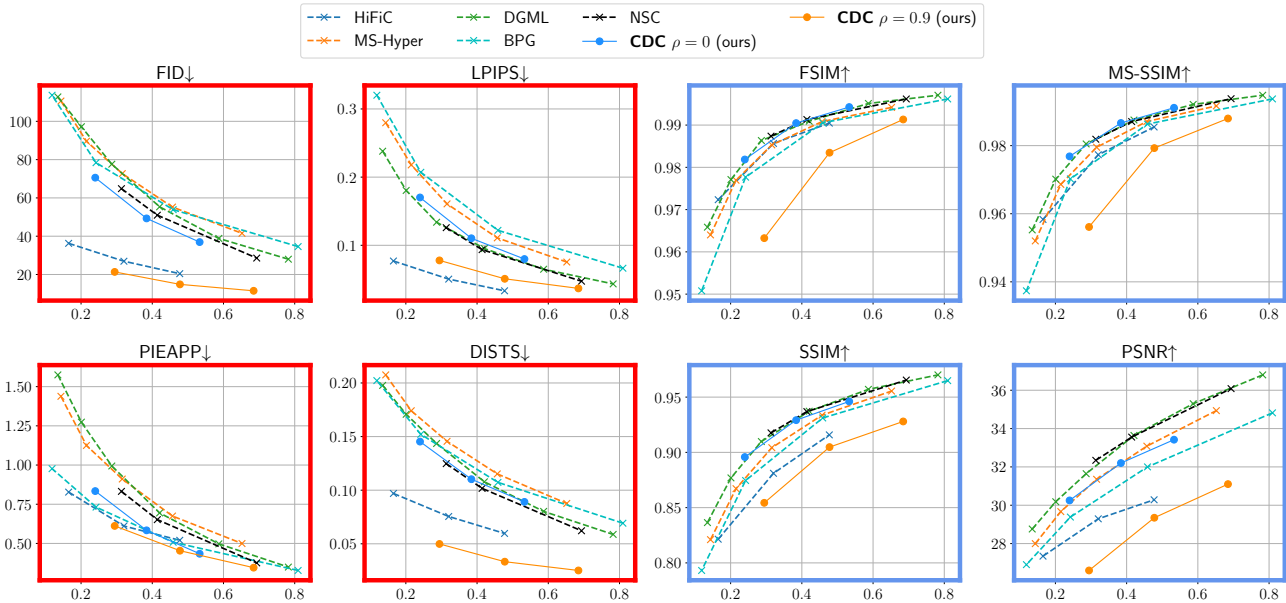


Figure 2: Tradeoffs between bitrate (x-axes, in bpp) and different metrics (y-axes) for various models tested on DIV2K. We consider both perceptual (red frames) and distortion metrics (blue frames). Arrows in the plot titles indicate whether high (\uparrow) or low (\downarrow) values indicate a better score. CDC (proposed) in its basic version (deterministic, without finetuning to LPIPS) compares favorably in distortion metrics, while CDC with stochastic decoding and added LPIPS losses performs favorably on perceptual metrics.

by an adversarial network and employs additional perceptual and traditional distortion losses (LPIPS and MSE). In terms of rate-distortion performance, two VAE models are selected: **DGML** (Cheng et al., 2020) and **NSC** (Wang et al., 2022). Both are the improvements over the MSE-trained Mean-Scale Hyperprior (**MS-Hyper**) architecture (Minnen et al., 2018). For a fair comparison, we did not use the content-adaptive encoding for NSC model. For comparisons with classical codecs, we choose **BPG** as a reference.

Figure 2 illustrates the tradeoff between bitrate and image quality using the DIV2K dataset. We only employ 17 steps to decode the images with \mathcal{X} -prediction model, which is much more efficient than ϵ -prediction model that requires hundreds of steps to achieve comparable performance (see Appendix I for results on other datasets and comparison with ϵ -prediction). In the figure, dashed lines represent the baseline models, while solid lines depict our proposed CDC models. The eight shown plots present two different types of metrics, distinguished by their respective frame colors.

- **Perceptual Metrics (red)**. The red subplots depict perceptual metrics that assess the compression for realism. Our findings reveal that our proposed CDC model ($\rho = 0.9$) achieves the best performance in three out of four metrics. The closest competitor is the HiFiC baseline. Notably, HiFiC demonstrates the highest score in LPIPS but exhibits suboptimal performance in all other metrics.

- **Distortion Metrics (blue)**. The blue subfigures present distortion-based metrics. We note that the CDC model with $\rho = 0$ produces relatively favorable results in distortion metrics, excluding PSNR. It shows on-par scores with the best baselines in FSIM, SSIM, and MS-SSIM scores, despite none of the shown models being specifically optimized for these three metrics. In contrast, "classical" neural compression models (Minnen et al., 2018; Wang et al., 2022; Cheng et al., 2020) directly target MSE distortion by minimizing an ELBO objective with Gaussian decoders, resulting in better PSNR scores.

Our proposed versions CDC ($\rho=0$) and CDC ($\rho=0.9$) show qualitative differences in perceptual and distortion metrics. Setting $\rho = 0$ only optimizes a trade-off between bitrate and the diffusion loss; compared to $\rho = 0.9$, this results in better performance in model-based distortion metrics (i.e., except PSNR). Fig. 3 qualitatively shows that the resulting decoded images show fewer over-smoothing artifacts than VAE-based codecs (Cheng et al., 2020). In contrast, CDC ($\rho=0.9$) performs the best in perceptual metrics. These are often based on extracted neural network features, such as Inception or VGG (Szegedy et al., 2016; Simonyan & Zisserman, 2014), and are more susceptible to image realism. By varying ρ , we can hence control a three-way trade-off among distortion, perceptual quality, and bitrate (See Appendix F for results with other ρ values).

References

- Agustsson, E. and Timofte, R. Ntire 2017 challenge on single image super-resolution: Dataset and study. In *The IEEE Conference on Computer Vision and Pattern Recognition (CVPR) Workshops*, July 2017.
- Agustsson, E., Tschannen, M., Mentzer, F., Timofte, R., and Gool, L. V. Generative adversarial networks for extreme learned image compression. In *Proceedings of the IEEE/CVF International Conference on Computer Vision*, pp. 221–231, 2019.
- Asuni, N. and Giachetti, A. Testimages: a large-scale archive for testing visual devices and basic image processing algorithms, stag - smart tools & apps for graphics conference, 2014. 2014.
- Ballé, J., Minnen, D., Singh, S., Hwang, S. J., and Johnston, N. Variational image compression with a scale hyperprior. *International Conference on Learning Representations*, 2018.
- Bégaint, J., Racapé, F., Feltman, S., and Pushparaja, A. Compressai: a pytorch library and evaluation platform for end-to-end compression research. *arXiv preprint arXiv:2011.03029*, 2020.
- Blau, Y. and Michaeli, T. Rethinking lossy compression: The rate-distortion-perception tradeoff. In *International Conference on Machine Learning*, pp. 675–685. PMLR, 2019.
- Brock, A., Donahue, J., and Simonyan, K. Large scale gan training for high fidelity natural image synthesis. In *International Conference on Learning Representations*, 2019.
- Cheng, Z., Sun, H., Takeuchi, M., and Katto, J. Learned image compression with discretized gaussian mixture likelihoods and attention modules. In *Proceedings of the IEEE/CVF Conference on Computer Vision and Pattern Recognition*, pp. 7939–7948, 2020.
- Cisco. Visual network index cisco. forecast and methodology. *White Paper*, 2017.
- Ding, K., Ma, K., Wang, S., and Simoncelli, E. P. Image quality assessment: Unifying structure and texture similarity. *IEEE transactions on pattern analysis and machine intelligence*, 2020.
- Dosovitskiy, A. and Brox, T. Generating images with perceptual similarity metrics based on deep networks. *Advances in neural information processing systems*, 29, 2016.
- Franzen, R. W. True color kodak images. 2013. URL <http://r0k.us/graphics/kodak/>.
- He, K., Zhang, X., Ren, S., and Sun, J. Deep residual learning for image recognition. In *Proceedings of the IEEE conference on computer vision and pattern recognition*, pp. 770–778, 2016.
- Heusel, M., Ramsauer, H., Unterthiner, T., Nessler, B., and Hochreiter, S. Gans trained by a two time-scale update rule converge to a local nash equilibrium. *Advances in neural information processing systems*, 30, 2017.
- Ho, J., Jain, A., and Abbeel, P. Denoising diffusion probabilistic models. *Advances in Neural Information Processing Systems*, 33:6840–6851, 2020.
- Kingma, D. P. and Ba, J. Adam: A method for stochastic optimization. *arXiv preprint arXiv:1412.6980*, 2014.
- Kuznetsova, A., Rom, H., Alldrin, N., Uijlings, J., Krasin, I., Pont-Tuset, J., Kamali, S., Popov, S., Mallocci, M., Kolesnikov, A., Duerig, T., and Ferrari, V. The open images dataset v4: Unified image classification, object detection, and visual relationship detection at scale. *IJCV*, 2020.
- Lin, T.-Y., Maire, M., Belongie, S., Hays, J., Perona, P., Ramanan, D., Dollár, P., and Zitnick, C. L. Microsoft coco: Common objects in context. In *European conference on computer vision*, pp. 740–755. Springer, 2014.
- Mentzer, F., Toderici, G. D., Tschannen, M., and Agustsson, E. High-fidelity generative image compression. *Advances in Neural Information Processing Systems*, 33:11913–11924, 2020.
- Minnen, D. and Singh, S. Channel-wise autoregressive entropy models for learned image compression. In *2020 IEEE International Conference on Image Processing (ICIP)*, pp. 3339–3343. IEEE, 2020.
- Minnen, D., Ballé, J., and Toderici, G. D. Joint autoregressive and hierarchical priors for learned image compression. *Advances in neural information processing systems*, 31, 2018.
- Prashnani, E., Cai, H., Mostofi, Y., and Sen, P. Pieapp: Perceptual image-error assessment through pairwise preference. In *Proceedings of the IEEE Conference on Computer Vision and Pattern Recognition*, pp. 1808–1817, 2018.
- Preechakul, K., Chatthee, N., Wizadwongsa, S., and Suwanajakorn, S. Diffusion autoencoders: Toward a meaningful and decodable representation. In *IEEE Conference on Computer Vision and Pattern Recognition (CVPR)*, 2022.
- Salimans, T. and Ho, J. Progressive distillation for fast sampling of diffusion models. In *International Conference on Learning Representations*, 2022.

- 275 Simonyan, K. and Zisserman, A. Very deep convolutional
276 networks for large-scale image recognition. *arXiv*
277 *preprint arXiv:1409.1556*, 2014.
- 278 Song, J., Meng, C., and Ermon, S. Denoising diffusion
279 implicit models. In *International Conference on Learning*
280 *Representations*, 2021a.
- 282 Song, Y. and Ermon, S. Generative modeling by estimating
283 gradients of the data distribution. *Advances in Neural*
284 *Information Processing Systems*, 32, 2019.
- 286 Song, Y., Sohl-Dickstein, J., Kingma, D. P., Kumar, A., Er-
287 mon, S., and Poole, B. Score-based generative modeling
288 through stochastic differential equations. In *International*
289 *Conference on Learning Representations*, 2021b.
- 291 Szegedy, C., Vanhoucke, V., Ioffe, S., Shlens, J., and Wojna,
292 Z. Rethinking the inception architecture for computer vi-
293 sion. In *Proceedings of the IEEE conference on computer*
294 *vision and pattern recognition*, pp. 2818–2826, 2016.
- 295 Wang, D., Yang, W., Hu, Y., and Liu, J. Neural data-
296 dependent transform for learned image compression. In
297 *Proceedings of the IEEE/CVF Conference on Computer*
298 *Vision and Pattern Recognition*, pp. 17379–17388, 2022.
- 300 Wang, Z., Bovik, A. C., and Simoncelli, E. P. Structural
301 approaches to image quality assessment. *Handbook of*
302 *image and video processing*, 7(18), 2005.
- 304 Xue, T., Chen, B., Wu, J., Wei, D., and Freeman, W. T.
305 Video enhancement with task-oriented flow. *International*
306 *Journal of Computer Vision (IJCV)*, 127(8):1106–1125,
307 2019.
- 308 Yang, Y., Bamler, R., and Mandt, S. Improving inference
309 for neural image compression. *Advances in Neural Infor-*
310 *mation Processing Systems*, 33:573–584, 2020.
- 312 Yang, Y., Mandt, S., and Theis, L. An introduction to neural
313 data compression. *Foundations and Trends in Computer*
314 *Graphics and Vision*, 2023.
- 316 Zhang, R., Isola, P., Efros, A. A., Shechtman, E., and Wang,
317 O. The unreasonable effectiveness of deep features as a
318 perceptual metric. In *Proceedings of the IEEE conference*
319 *on computer vision and pattern recognition*, pp. 586–595,
320 2018.
- 321 Zhao, S., Song, J., and Ermon, S. Towards deeper un-
322 derstanding of variational autoencoding models. *arXiv*
323 *preprint arXiv:1702.08658*, 2017.
- 325 Zheng, H., Nie, W., Vahdat, A., Azizzadenesheli, K., and
326 Anandkumar, A. Fast sampling of diffusion models
327 via operator learning. *arXiv preprint arXiv:2211.13449*,
328 2022.
- 329
- Zhu, Y., Yang, Y., and Cohen, T. Transformer-based trans-
form coding. In *International Conference on Learning*
Representations, 2021.

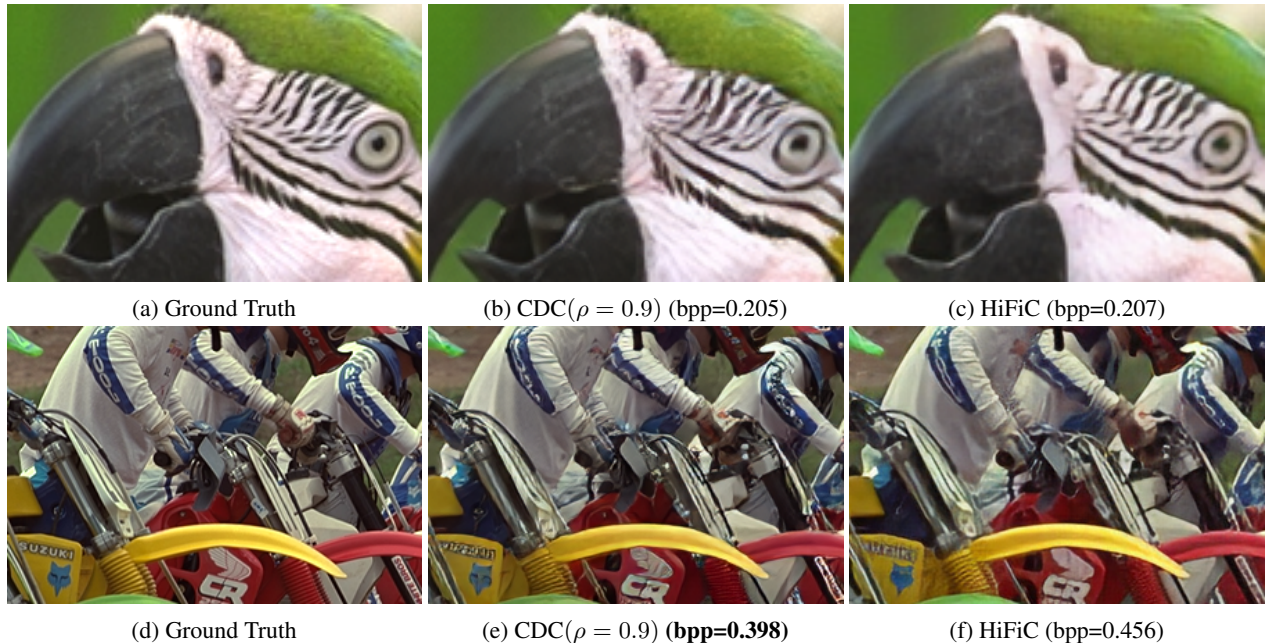


Figure 3: Reconstructed Kodak images (cropped images, see full images in Appendix G). 1st row: compared to HiFiC under similar bitrate, our model retains more details around the eyes of the parrot. 2nd row: our model still gets slightly better visual reconstruction than HiFiC while using *less* bitrate.

A. Supplemental Experiment Details

Metrics We selected sixteen metrics for image quality evaluations, of which we present eight most widely-used ones in the main paper and the remaining eight in the appendix. Specifically, several more recently proposed learned metrics (Heusel et al., 2017; Zhang et al., 2018; Prashnani et al., 2018; Ding et al., 2020) capture perceptual properties/realism better than other non-learned methods; we denote these metrics as *perceptual metrics* and the others as *distortion metrics*. It is important to note that when calculating FID, we follow Mentzer et al. (2020) by segmenting images into non-overlapping patches of 256×256 resolution.

Test Data To support our compression quality assessment, we consider the following datasets with necessary preprocessing: **1. Kodak** (Franzen, 2013): The dataset consists of 24 high-quality images at 768×512 resolution. **2. Tecnick** (Asuni & Giachetti, 2014): We use 100 natural images with 600×600 resolutions and then downsample these images to 512×512 resolution. **3. DIV2K** (Agustsson & Timofte, 2017): The validation set of this dataset contains 100 high-quality images. We resize the images with the shorter dimension being equal to 768px. Then, each image is center-cropped to a 768×768 squared shape. **4. COCO2017** (Lin et al., 2014): For this dataset, we extract all test images with resolutions higher than 512×512 and resize them to 384×384 resolution to remove compression artifacts. The resulting dataset consists of 2695 images.

Model Training We use the **Vimeo-90k** (Xue et al., 2019) dataset to train our model, consisting of 90,000 clips of 7-frame sequences at 448×256 resolution collected from vimeo.com. This dataset is widely used for video compression research. We select one frame from each clip and crop the frame randomly to 256×256 resolution. At the beginning of training, we warm up the model by setting $\lambda = 10^{-5}$ and keep it running for around 500,000 steps. Then, we increase λ to match the desired bitrates and keep the model running for another 1,000,000 steps until the model converges. We use $N_{\text{train}} = 20000$ for ϵ -prediction model and $N_{\text{train}} = 8000$ for \mathcal{X} -prediction model. The batch_size is set as 4, and the Adam (Kingma & Ba, 2014) optimizer is used. The learning rate is initialized as $lr = 5 \times 10^{-5}$ and then declines by 20% every 100,000 steps until $lr = 2 \times 10^{-5}$.

Distortion vs. Perception Our experiments revealed the aforementioned distortion-perception tradeoff in learned compression (Blau & Michaeli, 2019). In contrast to perceptual metrics, distortions such as PSNR are very sensitive to imperceptible image translations (Wang et al., 2005). The benefit of distortions is that they carry out a direct comparison

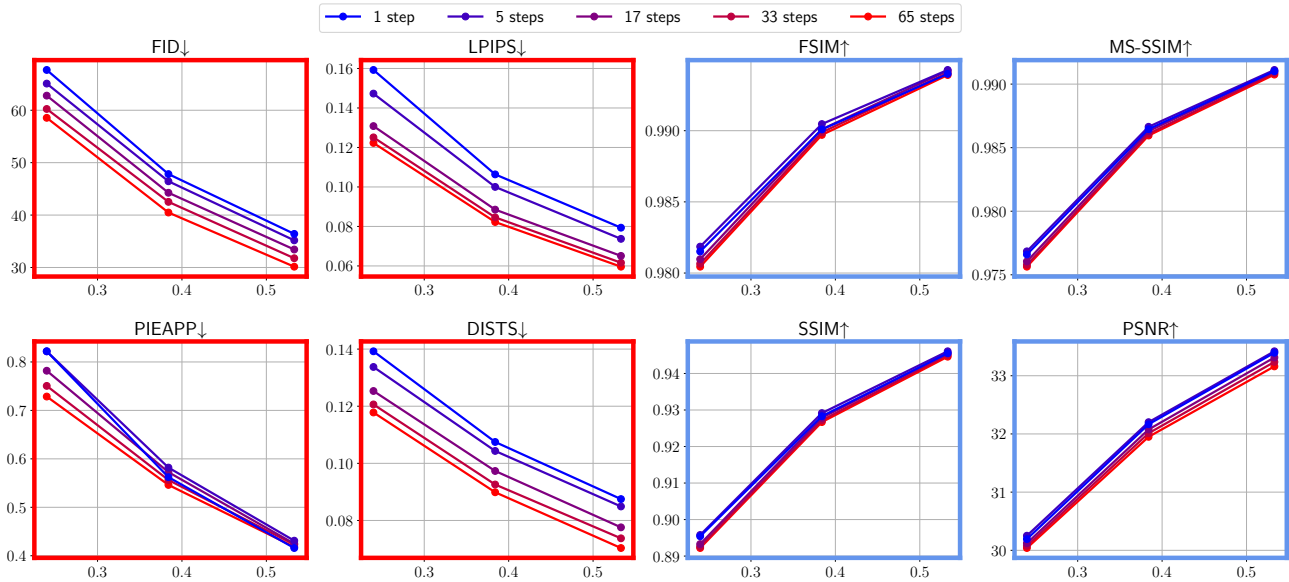


Figure 4: Compression performance with different numbers of decoding step. We use $\gamma = 0$ (deterministic decoding) to plot distortion curves and $\gamma = 1$ for perceptual quality curves.

between the reconstructed and original image, albeit using a debatable metric (Dosovitskiy & Brox, 2016). The question of whether distortion or perceptual quality is more relevant may ultimately not be easily solvable; yet it is plausible that most compression gains can be expected when targeting a combination of perception/realism and distortion, rather than distortion alone (Mentzer et al., 2020; Yang et al., 2023). Especially, our method’s strong performance in terms of FID, one of the most widely-adopted perceptual evaluation schemes (Ho et al., 2020; Song & Ermon, 2019; Mentzer et al., 2020; Brock et al., 2019; Song et al., 2021a;b), seems promising in this regard.

A.1. Ablation Studies

Influence of decoding steps In the previous section, we demonstrated that the CDC \mathcal{X} -prediction model can achieve decent performance with a small number of decoding steps. In Figure 4, we further investigate the compression performance of the \mathcal{X} -prediction($\rho = 0$) model using different decoding steps. Our findings reveal that when employing stochastic decoding, the model consistently produces better *perceptual* results as the number of decoding steps increases. However, in the case of deterministic decoding, more decoding steps do not lead to a substantial improvement in *distortion*.

Our findings show that the \mathcal{X} -prediction model can behave similarly to a Gaussian VAE decoder. In this scenario, the latent code \mathbf{z} becomes the primary determinant of the decoding outcome, enabling the model to reconstruct the original image \mathbf{x}_0 with a single decoding step. However, even a single decoding step has a tendency to reconstruct data closer to the data mode, only guaranteeing an acceptable distortion score. To effectively improve perceptual quality, it is crucial to incorporate more iterative decoding steps, particularly when utilizing stochastic decoding. Thus, we further explore the impact of stochastic decoding through the following ablation experiment.

Stochastic Decoding By adjusting the noise level parameter, denoted as γ , during the image decoding process, we can achieve different decoding outcomes. In order to investigate the impact of the noise on the decoding results, we present Figure 5, which provides both quantitative and qualitative evidence for 4 candidate γ values. Our findings indicate that larger values lead to improved perceptual quality and higher distortion, as evidenced by lower LPIPS and lower MS-SSIM. Values of γ greater than 0.8 not only increase distortion but also diminish perceptual quality. In terms of finding the optimal balance, a γ value of 0.8 offers the lowest LPIPS and the best qualitative outcomes as shown in Figure 5. From a qualitative standpoint, we notice that the noise introduces plausible high-frequency textures. Although these textures may not perfectly match the uncompressed ones (which is impossible), they are visually appealing when an appropriate γ is chosen. For additional insights into our decoding process, we provide visualizations of the decoding steps in Appendix H. These visualizations showcase how “texture” variables evolve during decoding.



Figure 5: Qualitative comparison of deterministic and stochastic decoding methods. Deterministic decoding typically results in a smoother image reconstruction. By increasing the noise γ used upon decoding the images, we observe more and more detail and rugged texture on the face of the sculpture. ($\gamma = 0.8$) show the best agreement with the ground truth image. All the images share the same bpp.

B. Pretrained Baselines

We refer to Bégaint et al. (2020) for pretrained MS-Hyper and DGML models. For HiFiC model, we use the pretrained models implemented in the publicly available repositories¹. Both models were sufficiently trained on natural image datasets (Xue et al., 2019; Kuznetsova et al., 2020). For NSC (Wang et al., 2022) baseline, we use the official codebase² and DIV2k training dataset to train the model.

C. Architectures

The design of the denoising module follows a similar U-Net architecture used in DDIM (Song et al., 2021a) and DDPM (Ho et al., 2020) projects. Each U-Net unit includes two ResNet blocks (He et al., 2016), one attention block and a convolutional up/downsampling block. We use six U-Net units for both downsampling and upsampling process. The channel dimension for each downsampling unit is $64 \times j$, where j is the index of the layer range from 1 to 6; the upsampling units follow the reverse order. Each encoder module consists of one ResNet block and one convolutional downsampling block. For conditioning with embedding, we use ResNet blocks and transposed convolution to upscale \mathbf{z} to the same spatial dimension as the inputs of the beginning four U-Net downsampling units, so that we can perform conditioning by concatenating the the output of the embedder and the input of the corresponding U-Net unit.

Figure 6 also describes our design choice of the model. We list the additional detailed specifications that we did not clarify in the main paper as follow:

- The hyper prior structure shares the same design as Minnen et al. (2018). The channel number of the hyper latent \mathbf{y} is set as 256.
- We use 3x3 convolution for most of the convolutional layers. The only exceptions are the 1st conv-layer of the first DU component and the 1st layer of the 1st ENC component, where we use 7x7 convolution for wider receptive field.
- i_N^n is embedded by a linear layer, which expand the 1-dimensional scalar to the same channel size as the corresponding DU/UU units. We then add the expanded tensor to the intermediate ResBlock of each DU/UU unit.

¹<https://github.com/Justin-Tan/high-fidelity-generative-compression>

²<https://github.com/Dezhao-Wang/Neural-Syntax-Code>

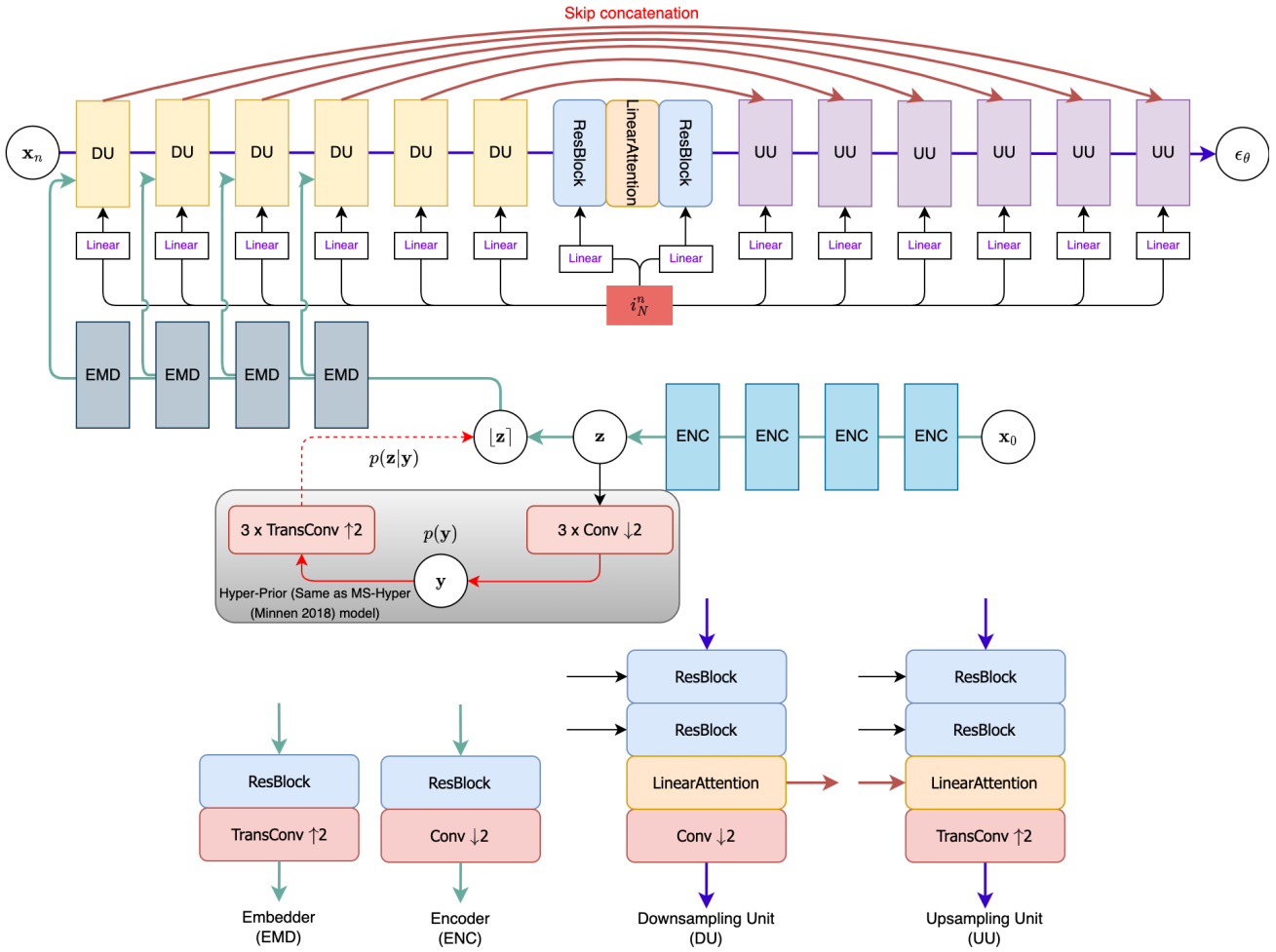


Figure 6: Visualization of our model architecture

D. Compute

We provide information on the model parameter size of the proposed model and baselines, and the corresponding time cost of running a full forward pass in Table 1. We run benchmarking on a server with a RTX A6000. We decode 24 images from Kodak dataset and calculate the average neural decoding time, which does not include entropy-coding process.

	CDC (1 step)	CDC (17 steps)	HiFiC	MS-hyper	DGML
Number of Parameters	53.8M	53.8M	181.47M	17.5M	26.5M
Decoding Time (Seconds)	0.015	1.04	0.0051	0.0011	0.0025

Table 1: Model and decoding time.

Our model exhibits superior memory efficiency compared to HiFiC. However, diffusion models suffer from slow decoding speed owing to their iterative denoising process. In the benchmark model utilized in our main paper, the decoding of an image takes approximately 1 second. Although this is slower than the baselines, it remains within an acceptable time range. Further optimization of the neural network module, such as the removal of the attention module, holds the potential to enhance efficiency even further.

E. Additional explanation on experiment metrics

FID, as the most popular metric for evaluating the *realism* of images, measures the divergence (Fréchet Distance) between the statistical distributions of compressed image latent features and ground truth ones. The model extracts features from Inception network and calculates the latent features' corresponding mean and covariance. **LPIPS** measures the l2 distance between two latent embeddings from VGG-Net/AlexNet. Likewise, **PieAPP** provides a different measurement of perceptual score based on a model that is trained with the pairwise probabilities. **DISTS** measures the structural and textural similarities based on multiple layers of network feature maps and an algorithm inspired by SSIM. **CKDN** leverages a distillation method that can extract a knowledge distribution from reference images, which can help calculate the likelihood of the restored image under such distribution. Both **MUSIQ** and **DBCNN** are non-reference metrics, as they both use deep network models (transformer and CNN, respectively) that are pre-trained on labeled image data with Mean Opinion Score. For non-learned metrics (model-based methods), **FSIM** uses the phase congruency and the color gradient magnitude of two images to calculate the similarity. The **(CW/MS-)SSIM** family uses insights about human perception of contrasts to construct a similarity metric to mimic human perception better. **GMSD** evaluates the distance between image color gradient magnitudes. **NLPD** means normalized Laplacian pyramid distance, which derives from a simple model of the human visual system and is also sensitive to the contrast of the images. **VSI** reflects a quantitative measure of visual saliency that is widely studied by psychologists and neurobiologists. **MAD** implements a multi-stage algorithm also inspired by the human visual system for distortion score calculation.

F. Supplemental Ablation Study

By varying the trade-off term ρ , we can train a model either prefer perceptual quality or traditional distortion performance. Figure 7 shows the rate-distortion curves for COCO dataset with the same decoding scheme. We consider four values in the study (0, 0.32, 0.64, 0.9). The result shows that larger ρ leads to better perceptual quality but worse distortions in most cases. We also note that $\rho > 0.9$ is not available as perceptual quality can not be perceivably improved and there is also a risk that the training may fail.

G. Additional visualization of the compressed images and decoding variability visualization

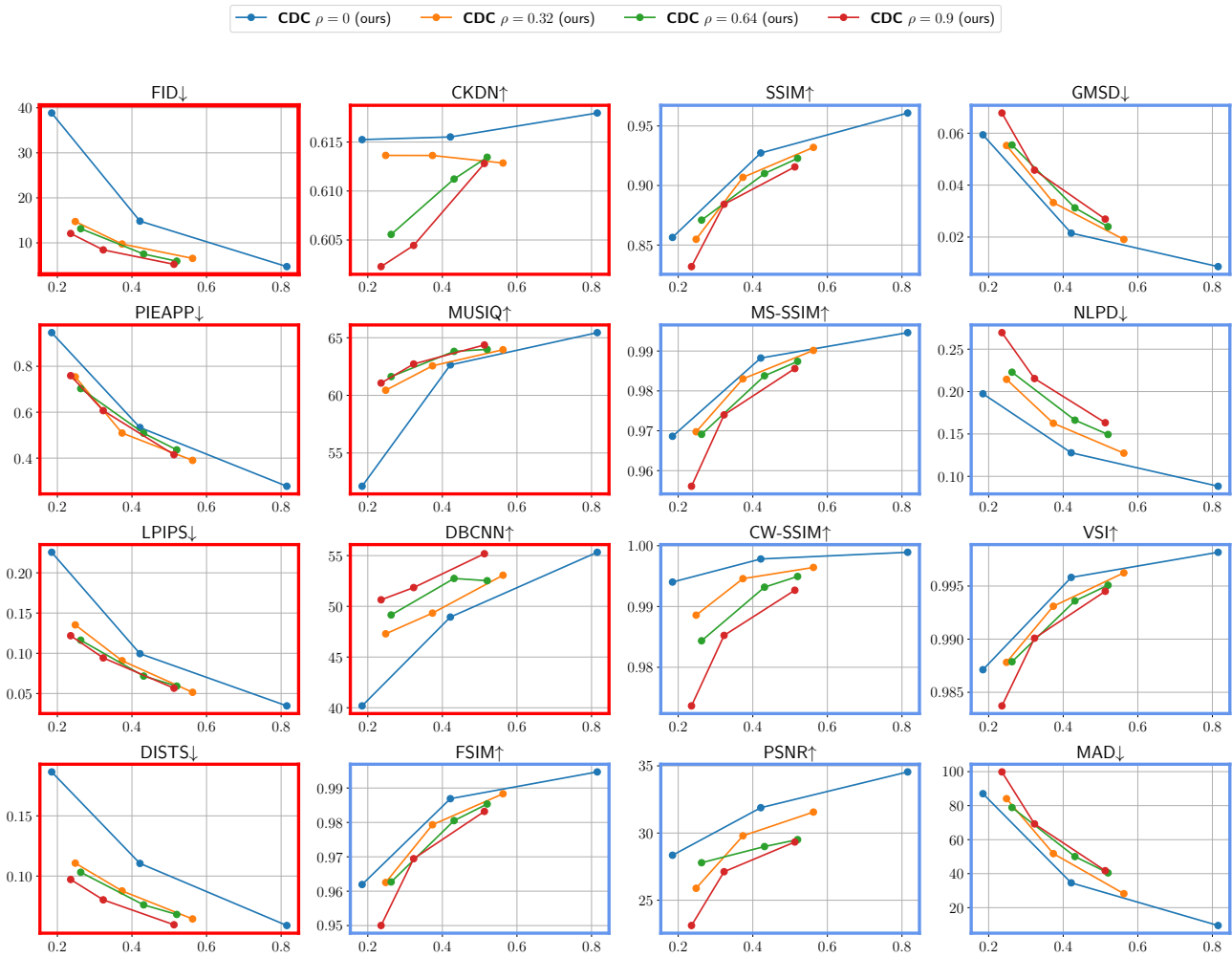


Figure 7: rate-distortion curves with different ρ values

660
661
662
663
664
665
666
667
668
669
670
671
672
673
674
675
676
677
678
679
680
681
682
683
684
685
686
687
688
689
690
691
692
693
694
695
696
697
698
699
700
701
702
703
704
705
706
707
708
709
710
711
712
713
714



Figure 8: Ground Truth

715
716
717
718
719
720
721
722
723
724
725
726
727
728
729
730
731
732
733
734
735
736
737
738
739
740
741
742
743
744
745
746
747
748
749
750
751
752
753
754
755
756
757
758
759
760
761
762
763
764
765
766
767
768
769



Figure 9: CDC $\mathcal{X}_\theta(\rho = 0.9)$, bpp=0.205

770
771
772
773
774
775
776
777
778
779
780
781
782
783
784
785
786
787
788
789
790
791
792
793
794
795
796
797
798
799
800
801
802
803
804
805
806
807
808
809
810
811
812
813
814
815
816
817
818
819
820
821
822
823
824



Figure 10: HiFiC bpp=0.207

825
826
827
828
829
830
831
832
833
834
835
836
837
838
839
840
841
842
843
844
845
846
847
848
849
850
851
852
853
854
855
856
857
858
859
860
861
862
863
864
865
866
867
868
869
870
871
872
873
874
875
876
877
878
879



Figure 11: Ground Truth

880
881
882
883
884
885
886
887
888
889
890
891
892
893
894
895
896
897
898
899
900
901
902
903
904
905
906
907
908
909
910
911
912
913
914
915
916
917
918
919
920
921
922
923
924
925
926
927
928
929
930
931
932
933
934



Figure 12: CDC $\mathcal{X}_\theta(\rho = 0.9)$, bpp=0.398

935
936
937
938
939
940
941
942
943
944
945
946
947
948
949
950
951
952
953
954
955
956
957
958
959
960
961
962
963
964
965
966
967
968
969
970
971
972
973
974
975
976
977
978
979
980
981
982
983
984
985
986
987
988
989



Figure 13: HiFiC bpp=0.456

990
 991
 992
 993
 994
 995
 996
 997
 998
 999
 1000
 1001
 1002
 1003
 1004
 1005
 1006
 1007
 1008
 1009
 1010
 1011
 1012
 1013
 1014
 1015
 1016
 1017
 1018
 1019
 1020
 1021
 1022
 1023
 1024
 1025
 1026
 1027
 1028
 1029
 1030
 1031
 1032
 1033
 1034
 1035
 1036
 1037
 1038
 1039
 1040
 1041
 1042
 1043
 1044



Figure 14: We stochastically decode the same latent variable \mathbf{z} and $\gamma = 0.8$ but different random seed for $\mathbf{x}_N \sim \mathcal{N}(\mathbf{0}, \gamma^2 \mathbf{I})$. Different random seeds may yield low-level textural distinction.

H. Visualizations of the Decoding Process



(a) A deterministic decoding scheme



(b) A stochastic decoding scheme

Figure 15: Comparing two decoding schemes with ϵ_θ parameterization for decoding the same image. The visualization showcases the texture variable \mathbf{x}_n at five different time steps ($n = \{0\%N, 30\%N, 60\%N, 90\%N, 100\%N\}$) using N decoding steps.

I. Additional Rate-Distortion(Perception) Results

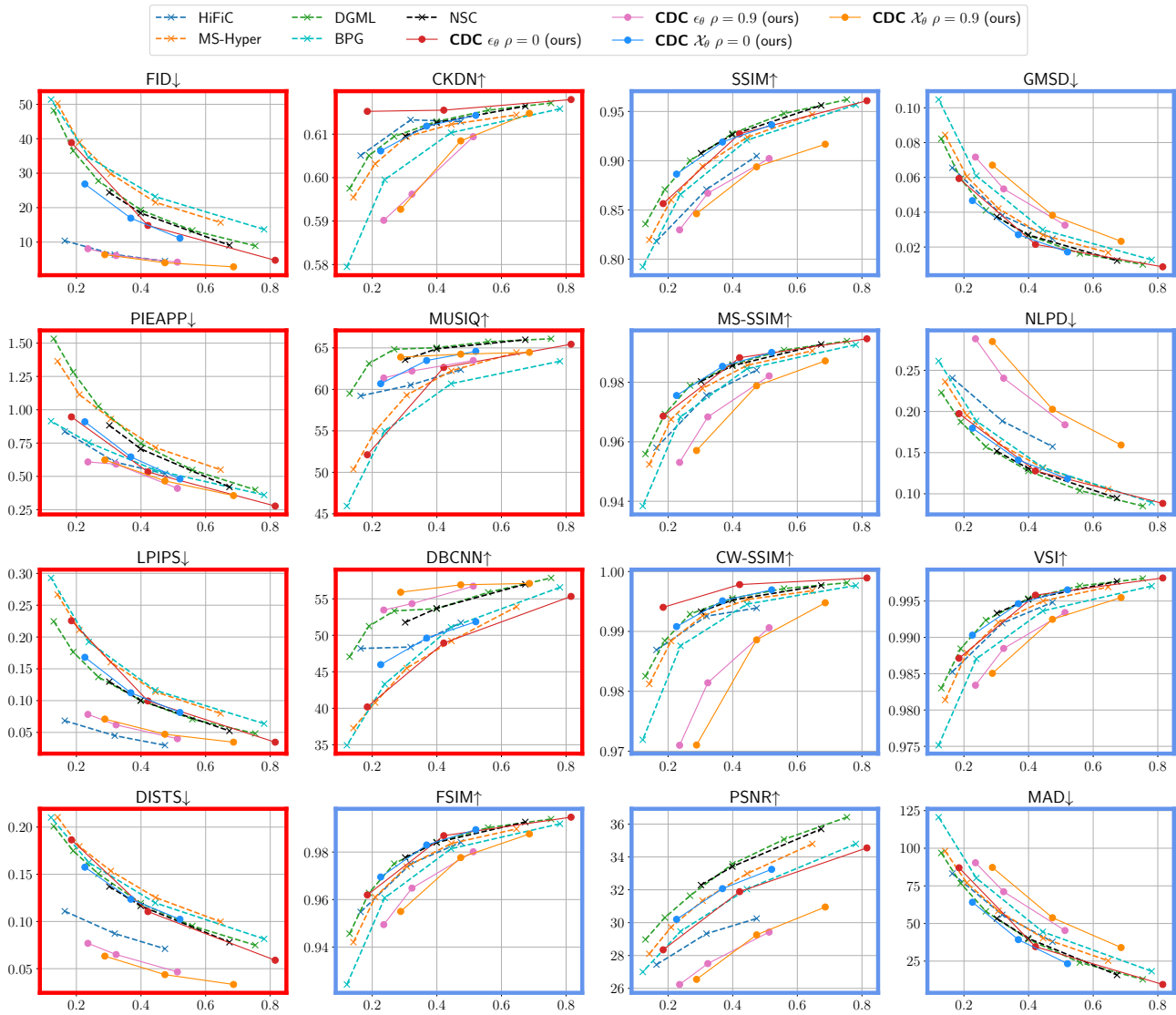


Figure 16: Rate-Distortion(Perception) for COCO dataset. We use 500 decoding steps for ϵ_θ model.

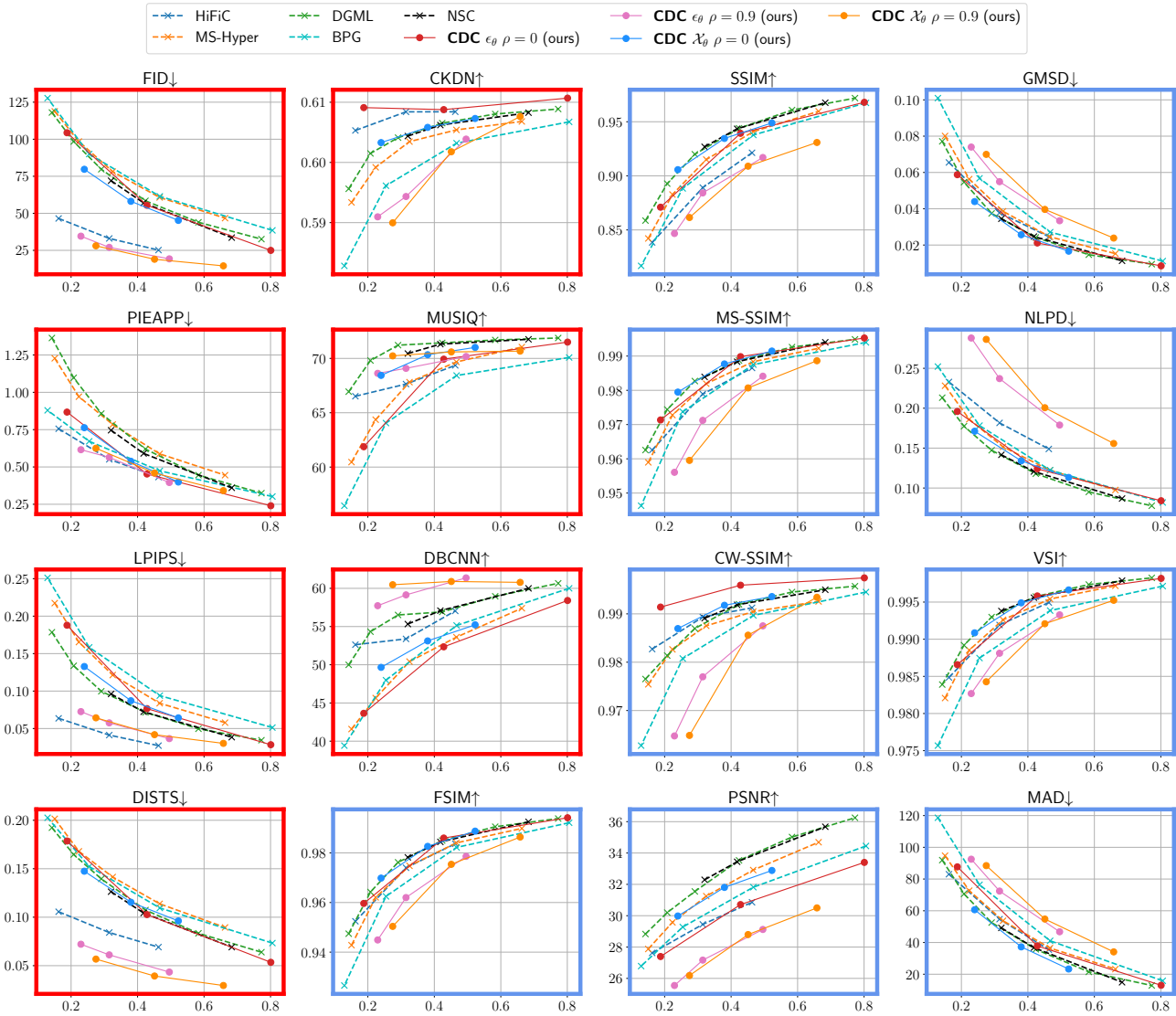


Figure 17: Rate-Distortion(Perception) for Tecnick dataset. We use 500 decoding steps for ϵ_θ model.

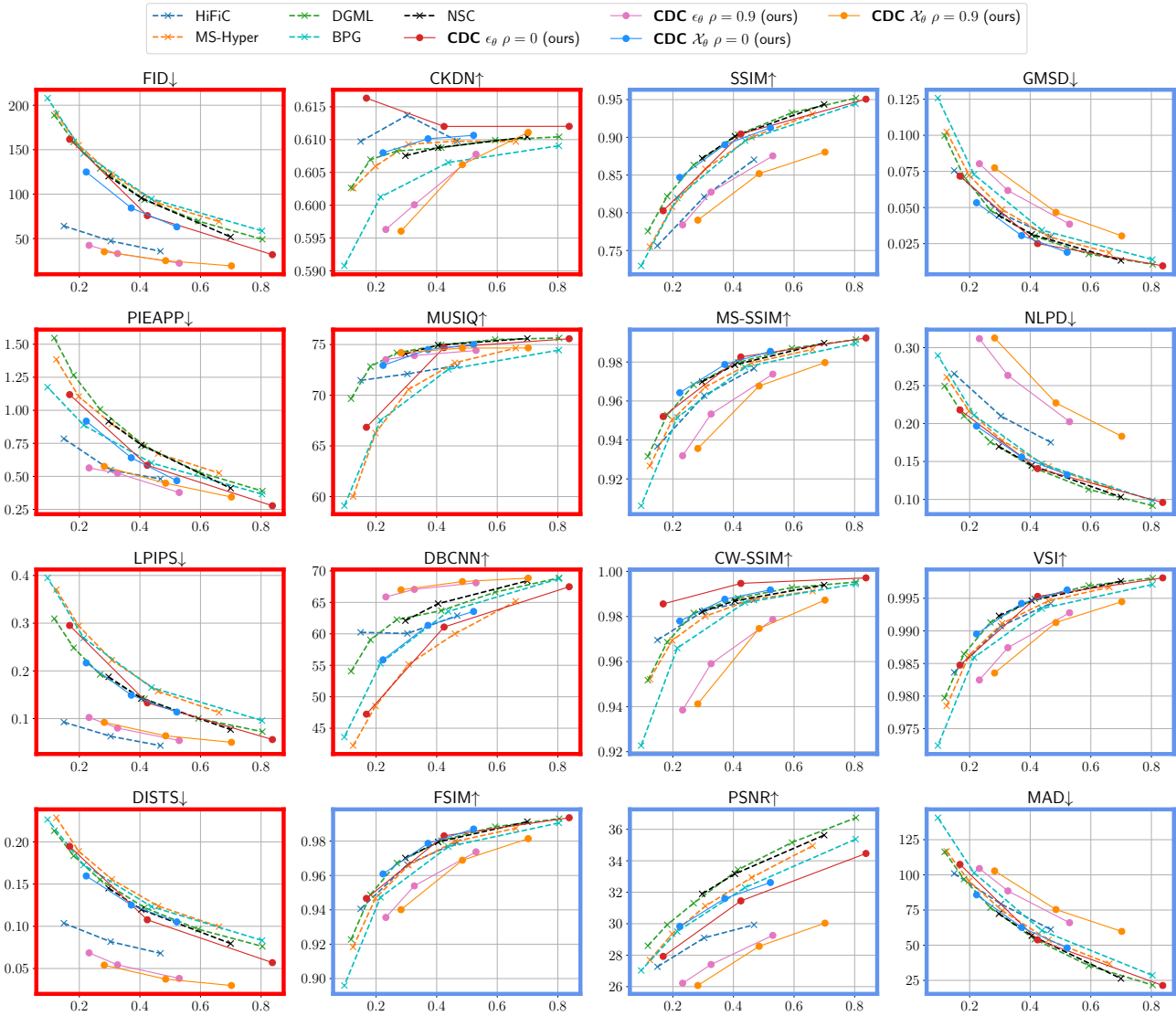


Figure 18: Rate-Distortion(Perception) for Kodak dataset. We use 500 decoding steps for ϵ_θ model.

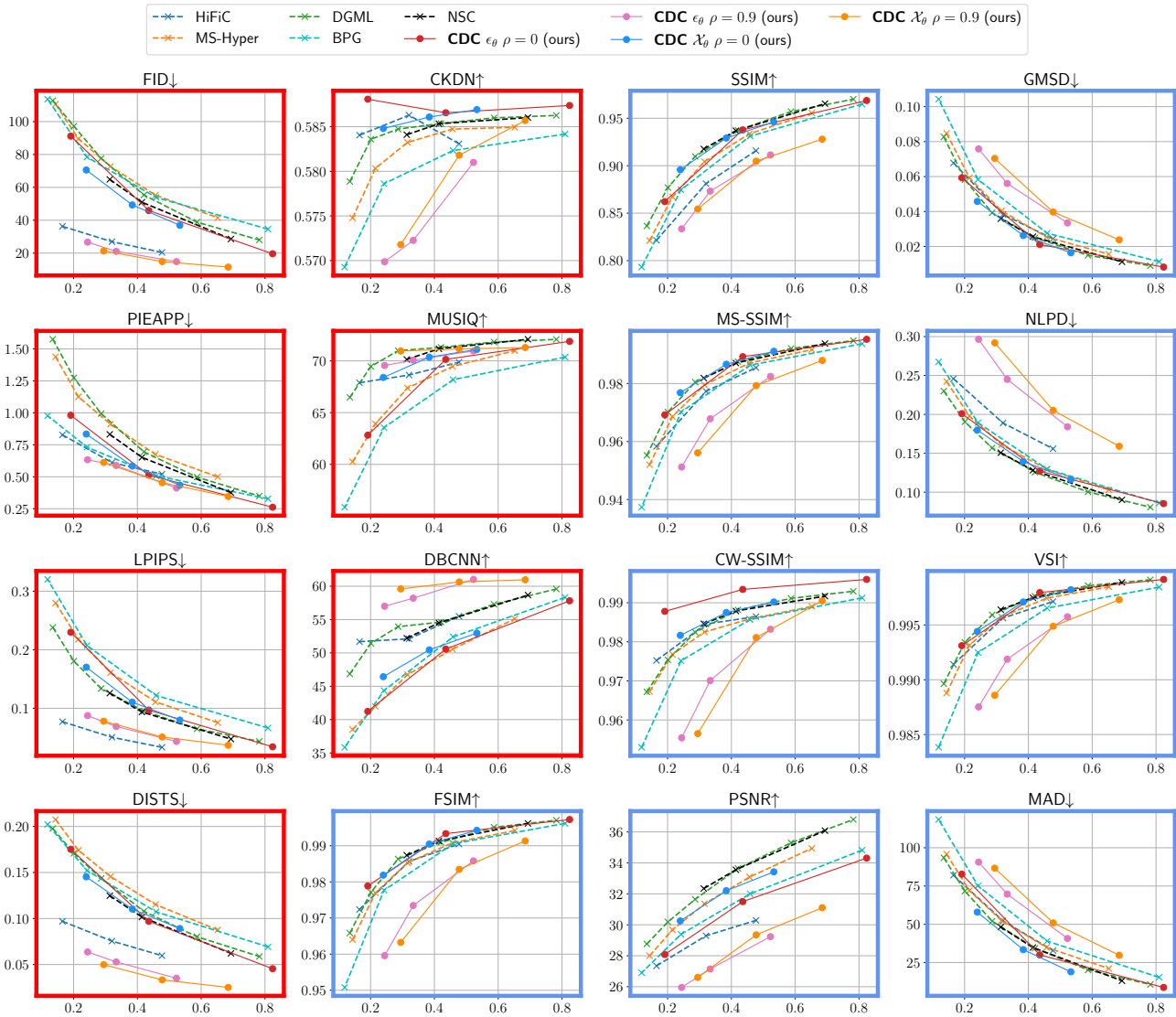


Figure 19: Rate-Distortion(Perception) for DIV2K dataset. We use 500 decoding steps for ϵ_θ model.. The complete 16 metrics.